Nanoengineered Catalyst Particles as a Key for Tailor-Made Carbon Nanotubes

Franziska Schäffel,*,† Christian Kramberger,† Mark H. Rümmeli,† Daniel Grimm,†,‡ Elias Mohn,† Thomas Gemming,† Thomas Pichler,† Bernd Rellinghaus,† Bernd Büchner,† and Ludwig Schultz†

IFW Dresden, P.O. Box 270116, D-01171 Dresden, Germany, and Instituto de Física, Universidade Federal Fluminense, Av. Gal. Milton Tavares de Souza s/n, 24210-346 Niterói-RJ, Brazil

Received April 5, 2007. Revised Manuscript Received August 1, 2007

Independent control of density and diameter of carbon nanotubes (CNT) is achieved by catalytic growth from iron nanoparticles pre-defined by inert gas condensation. This two-stage process offers the opportunity to investigate the particles prior to the CNT growth, thereby providing deeper insight into the growth mechanisms. The intimate correlation between particle and CNT diameters at particle densities, where interparticle coalescence is unavoidable, points to the nucleation of CNT setting in prior to this coalescence process.

Introduction

Owing to their unique mechanical and electronic properties,[1] carbon nanotubes (CNT) are promising candidates for applications such as components in compound materials,[2] field emitters for displays,[3] nanotube transistors,[4] and nanoelectromechanical systems such as nanorelays[5,6] or actuators.[7] Among the different CNT synthesis methods, chemical vapor deposition (CVD) is advantageous since it can be easily scaled up for mass production.[8] Furthermore, substrate-based CVD allows for the synthesis of aligned CNT[9] at defined positions[10−12] and thus holds significant potential for the integration of CNT into nanoelectronic devices. Here, the preparation of the catalyst material is a crucial step. Different approaches include wet chemistry[13,14] and the deposition of catalyst thin films onto substrates,[15−17] which can also be used for substrate patterning, e.g., by lithographical methods.[12,16] However, these routes have the drawback that the catalyst "particles" are formed in situ; hence, they do not afford simultaneous control over the catalyst areal density *and* the catalyst size together with a narrow diameter distribution. The simultaneous control though is the key to ensure the reliable and reproducible realization of CNT-based devices; hence, a technique which provides this control is of immense interest.

The preparation and deposition of individual pre-defined catalyst particles holds the potential to *independently* vary both the catalyst size and density. A relevant approach is, e.g., employing block-copolymer micellar thin films.[18] Catalyst particles in the nanometer regime are mainly synthesized by mechanical, chemical, or gas-phase preparation methods. Mechanical methods yield large quantities of material, but debris from the milling process causes impurities in the particles. Chemical methods can yield monodisperse particles which must then be separated by steric stabilizers. Gas-phase methods, on the other hand, allow for the synthesis of individual monodisperse particles in a single preparation step without the necessity to add stabilizers.

In this contribution, the controlled synthesis of CNT with defined diameters and densities via substrate-based CVD

* To whom correspondence should be addressed. E-mail: f.schaeffel@ifw-dresden.de.
† IFW Dresden.
‡ Universidade Federal Fluminense.

(1) Saito, R.; Dresselhaus, G.; Dresselhaus, M. S. *Physical Properties of Carbon Nanotubes*; Imperial College Press: London, 1998.
(2) Cadek, M.; Coleman, J. N.; Barron, V.; Hedicke, K.; Blau, W. *J. Appl. Phys. Lett.* **2002**, *81*, 5123−5125.
(3) Wang, Q. H.; Setlur, A. A.; Lauerhaas, J. M.; Dai, J. Y.; Seelig, E. W.; Chang, R. P. H. *Appl. Phys. Lett.* **1998**, *72*, 2912−2913.
(4) Bachtold, A.; Hadley, P.; Nakanishi, T.; Dekker, C. *Science* **2001**, *294*, 1317−1320.
(5) Lee, S. W.; Lee, D. S.; Morjan, R. E.; Jhang, S. H.; Sveningsson, M.; Nerushev, O. A.; Park, Y. W.; Campbell, E. E. B. *Nano Lett.* **2004**, *4*, 2027−2030.
(6) Cha, S. N.; Jang, J. E.; Choi, Y.; Amaratunga, G. A. J.; Kang, D.-J.; Hasko, D. G.; Jung, J. E.; Kim, J. M. *Appl. Phys. Lett.* **2005**, *86*, 803105.
(7) Fennimore, A. M.; Yuzvinsky, T. D.; Han, W.-Q.; Fuhrer, M. S.; Cumings, J.; Zettl, A. *Nature* **2003**, *424*, 408−410.
(8) Choi, G. S.; Cho, Y. S.; Son, K. H.; Kim, D. J. *Microelectron. Eng.* **2003**, *66*, 77−82.
(9) Ren, Z. F.; Huang, Z. P.; Xu, J. W.; Wang, J. H.; Bush, P.; Siegal, M. P.; Provencio, P. N. *Science* **1998**, *282*, 1105−1107.
(10) Kong, J.; Soh, H. T.; Cassell, A. M.; Quate, C. F.; Dai, H. *Nature* **1998**, *395*, 878−881.
(11) Kabir, M. S.; Morjan, R. E.; Nerushev, O. A.; Lundgren, P.; Bengtsson, S.; Enoksson, P.; Campbell, E. E. B. *Nanotechnology* **2006**, *17*, 790−794.
(12) Grimm, D.; Grüneis, A.; Kramberger, C.; Rümmeli, M. H.; Gemming, T.; Büchner, B.; Barreiro, A.; Kuzmany, H.; Pfeiffer, R.; Pichler, T. *Chem. Phys. Lett.* **2006**, *428*, 416−420.
(13) Maruyama, S.; Kojima, R.; Miyauchi, Y.; Chiashi, S.; Kohno, M. *Chem. Phys. Lett.* **2002**, *360*, 229−234.
(14) Hu, M.; Murakami, Y.; Ogura, M.; Maruyama, S.; Okubo, T. *J. Catal.* **2004**, *225*, 230−239.
(15) Delzeit, L.; Chen, B.; Cassell, A.; Stevens, R.; Nguyen, C.; Meyyappan, M. *Chem. Phys. Lett.* **2001**, *348*, 368−374.
(16) Hata, K.; Futaba, D. N.; Mizuno, K.; Namai, T.; Yumura, M.; Iijima, S. *Science* **2004**, *306*, 1362−1364.
(17) Grüneis, A.; Rümmeli, M. H.; Kramberger, C.; Barreiro, A.; Pichler, T.; Pfeiffer, R.; Kuzmany, H.; Gemming, T.; Büchner, B. *Carbon* **2006**, *44*, 3177−3182.
(18) Bennett, R. D.; Hart, A. J.; Cohen, R. E. *Adv. Mater.* **2006**, *18*, 2274−2279.

10.1021/cm070950k CCC: $37.00 © 2007 American Chemical Society
Published on Web 09/11/2007

from pre-defined gas-phase prepared iron particles is reported. The nanoparticle synthesis is achieved in a single step by sputtering from an elemental iron target. Thus, a higher degree of purity is obtained, as compared to processes where the synthesis of catalyst particles requires a series of chemical preparation steps.[18] The technique employed leads to individual and pure nanoparticles and affords facile control over particle size and density. With the appropriate choice of material, the deposited particles can act as nucleation sites for the growth of CNT in the subsequent CVD process. In addition, the separate generation of the catalyst particles facilitates their comprehensive characterization prior to the CVD process. This cannot be so conveniently accomplished in more conventional CVD methods[13−17] where the catalyst particles form in situ. Due to the ease with which detailed information on the catalysts' size distribution and dispersion can be accessed, the technique provides improved insight into the growth mechanisms of CNT. In the present study, this is highlighted by a direct relationship between the sizes of catalyst particles and of the resultant CNT diameters, respectively. Also, a clear link between the number of walls of the CNT and the catalyst size is established.

Experimental Section

The iron catalyst nanoparticles are prepared by inert-gas condensation based on magnetron sputtering from a pure Fe target in Ar and/or He atmosphere. For the CVD processing, the catalyst particles are deposited onto thermally oxidized silicon substrates coated with 10 nm thick Al_2O_3 layers. For transmission electron microscopy (TEM), particles are simultaneously deposited onto carbon-coated copper grids (referred to as TEM witness plates) mounted next to the CVD substrates. During any transfer of a particle sample from the deposition chamber into a microscope or into the CVD reactor, the particles are exposed to ambient air and thus oxidized. The subsequent CNT synthesis is carried out in a vertical high-vacuum CVD reactor. In the reaction, the particles are first reduced in hydrogen at 800 °C and then exposed to cyclohexane vapor. This method yields CNT material, which is ready for characterization without further purification.[19] Details of the nanoparticle deposition system, the CVD process, and the CVD reactor are described elsewhere.[20] The $Si/SiO_2/Al_3O_3$ support's surface dimensions were 1 cm × 0.5 cm. Typical yields for dense particle deposition were 50 μg (1 g/m^2) of CNT. CNT samples for TEM investigations are prepared by gently sliding an empty Cu grid over the CVD-processed substrate. Structural and morphological information are obtained by TEM on a FEI Tecnai F30 microscope and by scanning electron microscopy (SEM) on a FEI Nova NanoSem system. Raman spectroscopy of the CNT was conducted on a Bruker IFS100 spectrometer (1064 nm).

Results and Discussion

This gas-phase preparation route allows for the synthesis of very pure catalyst particles with a well-defined size distribution in a single step.[21] The mean particle size can be controlled by varying the sputtering power, the gas pressure, and/or the gas mixture. Different deposition times lead to different nanoparticle densities on the CVD substrates as shown in the TEM micrographs of the particle witness plates in Figures 1a−1c. Along with the particle density, the mean particle size d_P is varied in these samples (d_P = 5 nm, d_P = 7 nm, d_P = 10 nm in Figures 1a−1c, respectively). The corresponding SEM images (Figures 1d−1f) illustrate that low particle densities lead to isolated CNT (Figure 1d) and medium particle densities result in a coverage of the CVD substrate with rather interwoven CNT (Figure 1e), whereas high particle densities lead to the formation of dense CNT mats (Figure 1f). Figure 2 shows the Raman spectra of the as-grown CNT displayed in Figures 1d−1f. Raman lines originating from the silicon substrate (labeled "Si'') and those originating from the CNT, namely, the graphite mode ("G''), the defect mode ("D'') and the radial breathing modes ("RBMs''), are visible. For a low particle density (and size), the Raman spectrum (Figure 2a) shows a very weak CNT signal as compared to the silicon signal of the underlying substrate. Medium particle densities, as in the sample displayed in Figure 1b, lead to stronger G and D modes, and weak RBMs become visible (Figure 2b). For high particle densities (Figure 1f), the Raman response of the Si substrate is no longer detectable, whereas the RBMs from single-wall and possibly double-wall CNT are more distinct, although their intensity remains weak relative to the G mode

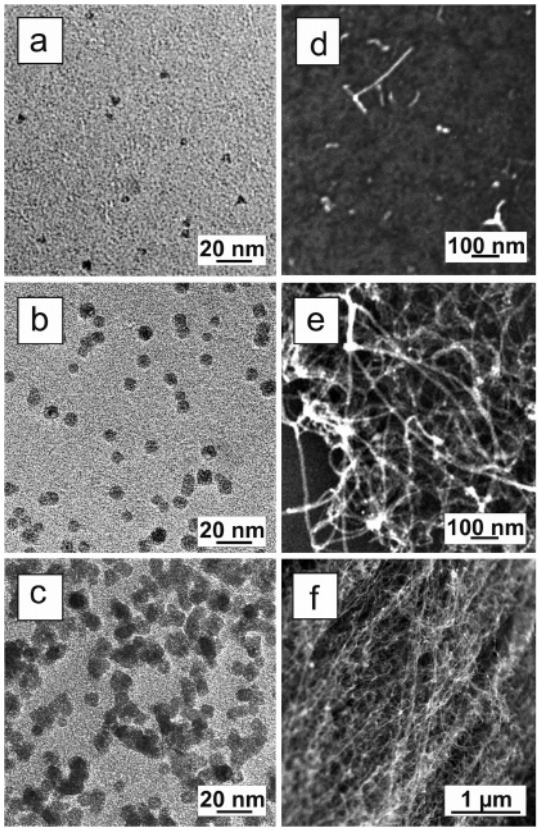

Figure 1. (a−c) TEM micrographs of (oxidized) Fe nanoparticles of varying size and density deposited onto amorphous carbon films. (d−f) SEM images of CNT grown from such particles on Al_2O_3-coated Si substrates via CVD.

(19) Grüneis, A.; Kramberger, C.; Grimm, D.; Gemming, T.; Rümmeli, M. H.; Barreiro, A.; Ayala, P.; Pichler, T.; Schaman, Ch.; Kuzmany, H.; Schumann, J.; Büchner, B. *Chem. Phys. Lett.* **2006**, *425*, 301−305.

(20) Schäffel, F.; Kramberger, C.; Rümmeli, M. H.; Kaltofen, R.; Grimm, D.; Grüneis, A.; Mohn, E.; Gemming, T.; Pichler, T.; Büchner, B.; Rellinghaus, B.; Schultz, L. *Phys. Status Solidi (a)* **2007**, *204*, 1786−1790.

(21) Stappert, S.; Rellinghaus, B.; Acet, M.; Wassermann, E. F. *J. Cryst. Growth* **2003**, *252*, 440−450.

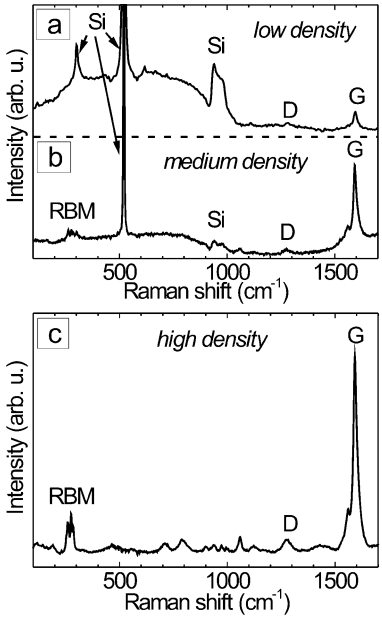

Figure 2. FT-Raman spectra (1064 nm) of the CNT samples displayed in Figures 1d−1f.

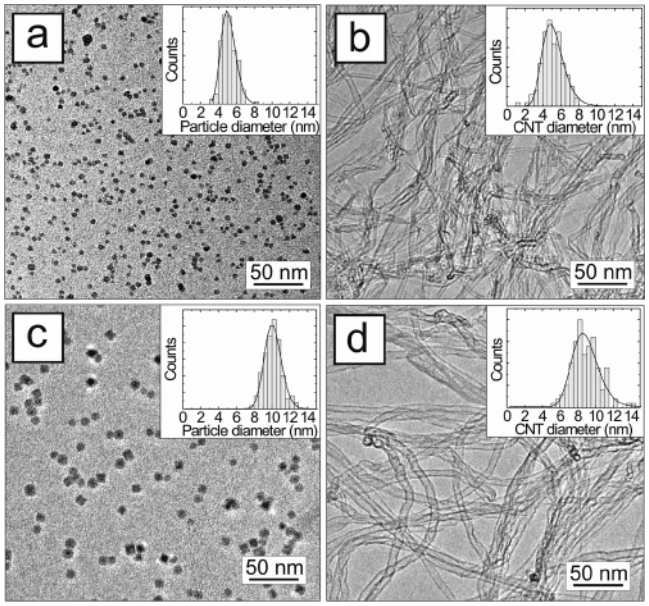

Figure 3. (a, c) TEM micrographs of (oxidized) Fe nanoparticles with median diameters of 5 and 10 nm, respectively. (b, d) Corresponding TEM micrographs of CNT grown from these particles. The particle size or CNT diameter distributions are shown as insets.

(Figure 2c). These changes in the Raman spectra confirm the intimate correlation between the density of the catalyst particles and the density of the CNT as seen from the TEM and SEM images. For all samples under investigation in this study, the Raman spectra show rather weak D lines with intensity ratios of the G and the D lines in the range $11 \leq I_G/I_D \leq 17$ which point to clean CNT with few defects. This demonstrates both the constantly high quality of the CNT samples and the homogeneity of the CVD process.

The effect of the catalyst particle size on the diameter of the resulting CNT is investigated with TEM. It is worth noting here that amorphous carbon contamination was *never* observed in any TEM studies of our CNT samples which again confirms the high purity of the obtained CNT material. Figure 3 shows TEM micrographs of catalyst particles with a median particle size of $d_P = 5$ nm and $d_P = 10$ nm (Figures 3a and 3c) together with images of the corresponding CNT samples (Figures 3b and 3d). The particle size and CNT diameter distributions, as measured from high-magnification TEM micrographs, are shown as insets in the images. As expected, all size distributions follow log-normal distribution functions.[22] The median diameters of the CNT are determined to be $d_{CNT} = 5$ nm and $d_{CNT} = 9$ nm, respectively; i.e., the particle sizes are in excellent agreement with the diameters of the obtained CNT. This indicates that the diameter of the catalyst particles dictates that of the resultant CNT which is in agreement with other studies on single-wall CNT.[23] Further statistical analyses reveal that the distributions of the CNT diameters are slightly broader than those of the particle diameters. The additional broadening arises mainly from CNT with diameters *smaller* than those of the particles. This finding is attributed to the size reduction of the catalyst particles during the hydrogen treatment prior to the CVD growth of CNT. The complete reduction of a thoroughly oxidized particle upon H_2 treatment would lead to a maximum shrinkage of the particle diameter of about 32% which is a reasonable upper limit for the observed effect and may well explain the observed shift of the median CNT diameter. At higher particle densities, an increase of the catalyst particle size due to coalescence is to be expected. However, investigations of samples with very high particle densities show that this has almost *no* effect on the diameters of the resultant CNT. Figures 4a and 4b show the starting catalyst particles and resultant CNT from a substrate with a very high particle density where most particles are in direct contact with other particles. The corresponding distributions of both the primary particle size and the CNT diameter are displayed in Figures 4d and 4e. Despite the obvious potential for particle coalescence at these densities, the median diameter of the obtained CNT ($d_{CNT} = 9$ nm) is in remarkably good agreement with the median *primary* particle diameter, $d_P = 10$ nm. Figure 4c shows a CNT with a diameter corresponding to the size of a single primary particle which is attached to a much larger coalesced particle agglomerate. This points to a scenario where the nucleation of the CNT sets in prior to particle coalescence: The coalescence of metal nanoparticles occurs largely via surface diffusion.[24] As soon as the catalytic growth of a CNT and hence the formation of a carbon layer around the *primary* catalyst particle are initiated, the surface diffusion on this particle is impeded or at least modified, and as a result, it may morphologically survive the ongoing coalescence of the particle agglomerate to which it belongs (cf. Figure 4f).

In addition to this templating nature of the catalyst, an intimate correlation between the catalyst particle size and the number of walls in the obtained CNT is observed. Figure 5 shows TEM micrographs of catalyst particles with a median

(22) Granqvist, C. G.; Buhrman, R. A. *J. Appl. Phys.* **1976**, *47*, 2200−2219.
(23) Li, Y.; Kim, W.; Zhang, Y.; Rolandi, M.; Wang, D.; Dai, H. *J. Phys. Chem. B* **2001**, *105*, 11424−11431.
(24) Tsyganov, S.; Kästner, J.; Rellinghaus, B.; Kauffeldt, T.; Westerholdt, F.; Wolf, D. *Phys. Rev. B* **2007**, *75*, 045421

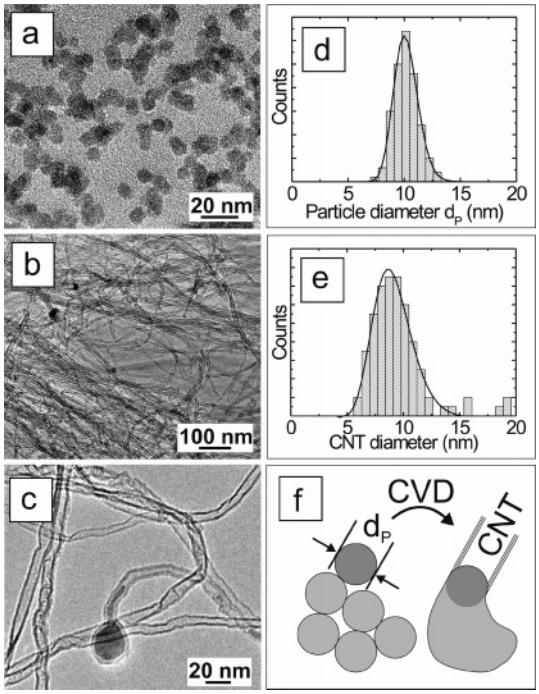

Figure 4. TEM micrographs of (a) dense Fe catalyst particles and (b,c) CNT grown from them. Corresponding (d) particle size and (e) CNT diameter distributions. (f) Schematic illustration of the CNT growth from agglomerated particles.

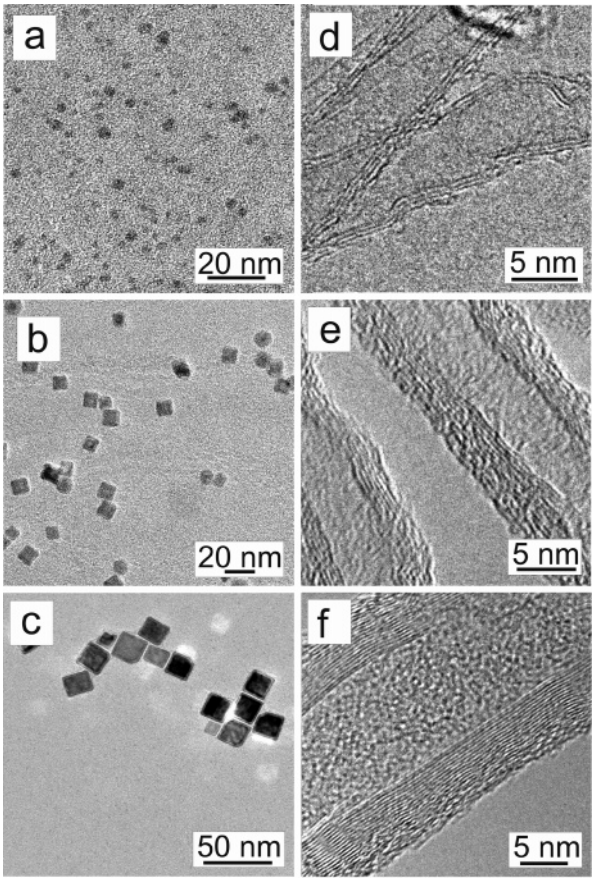

Figure 5. (a−c) TEM micrographs of the catalyst particles with median diameters of 2.7, 10, and 18 nm, respectively. (d−f) Corresponding HRTEM images of CNT grown from these particles.

particle size of $d_P = 2.7$ nm, $d_P = 10$ nm, and $d_P = 18$ nm (Figures 5a−5c) together with high-resolution images of the corresponding CNT (Figures 5d−5f). Detailed TEM studies show that the CVD processing of particles with a median diameter of $d_P = 2.7$ nm nucleate the growth of CNT with predominantly three walls (Figure 5d), whereas particles with a median diameter of $d_P = 10$ nm lead to the formation of multiwall CNT with 5−11 walls (Figure 5e). Increasing the particle size yet further to a median diameter of $d_P = 18$ nm yields CNT with 8−20 walls (Figure 5f). This correlation between the number of walls of a CNT and the catalyst *particle size* is in good agreement with other studies[25] where a correlation between different catalyst *film thicknesses* and both the obtained diameter and number of walls of the CNT was shown; the authors had attributed this finding to changes in the catalyst particle size. The separate preparation of the catalyst particles in our approach enables us to reveal a clear link between the catalyst *size* on the one side and the CNT diameter as well as the number of walls for a given set of CVD reaction parameters on the other side. This confirms a previously proposed CNT nucleation model[26,27] arguing that due to differences in the catalysts' volume-to-surface area, with increasing catalyst size the available carbon, which precipitates from the catalyst particle at the point of nucleation, can exceed the critical amount required for the formation of a single cap (the so-called embryonic stage of CNT growth). Hence, as the amount of precipitating carbon increases with the catalyst size, the number of walls that form the emerging CNT increases.

Conclusion

A gas-phase preparation method has been employed for the controlled one-step deposition of pure catalytic (oxidized) iron particles. When subjected to substrate-based CVD, these particles successfully nucleate and grow pure CNT material. The particle deposition time offers a facile means to predefine the density of nucleation sites and hence the amount of CNT, ranging from lone individual CNT to dense CNT mats. It is shown that the median diameter of the growing CNT is templated by the median particle size. This way of controlling the CNT diameter works for all investigated densities of catalyst particles since the coalescence-induced particle coarsening, which is unavoidable at high densities, apparently occurs only after the nucleation of the CNT. Further, we prove that as the catalysts particle size increases, so do the number of walls from the resultant CNT. The efficient control of our single-step catalyst particle preparation does not only yield a vital insight into CNT growth mechanisms but also truly offers tailored CNT.

Acknowledgment. F.S. acknowledges funding from the Cusanuswerk. C.K. thanks the International Max Planck Research School. T.P., M.H.R., and D.G. thank the DFG PI440/3-4 and the DAAD (grant Probral D/04/40433) for support.

CM070950K

(25) Yamada, T.; Namai, T.; Hata, K.; Futaba, D. N.; Mizuno, K.; Fan, J.; Yudasaka, M.; Yumura, M.; Iijima, S. *Nat. Nanotechnol.* **2006**, *1*, 131−136.
(26) Rümmeli, M. H.; Grüneis, A.; Löffler, M.; Jost, O.; Schönfelder, R.; Kramberger, C.; Grimm, D.; Gemming, T.; Barreiro, A.; Borowiak-Palen, E.; Kalbác, M.; Ayala, P.; Hübers, H.-W.; Büchner, B.; Pichler, T. *Phys. Status Solidi (b)* **2006**, *243*, 3101−3105.
(27) Rümmeli, M. H.; Kramberger, C.; Löffler, M.; Jost, O.; Bystrzejewski, M.; Grüneis, A.; Gemming, T.; Pompe, W.; Büchner, B.; Pichler, T. *J. Phys. Chem. B* **2007**, *111*, 8234−8241.